HHS Public Access

Author manuscript

Sci Transl Med. Author manuscript; available in PMC 2021 January 19.

Published in final edited form as:

Sci Transl Med. 2020 January 08; 12(525): . doi:10.1126/scitranslmed.aay4860.

Thrombin contributes to cancer immune evasion via proteolysis of platelet-bound GARP to activate LTGF-β

Alessandra Metelli[1], **Bill X. Wu**[2], **Brian Riesenberg**[2], **Silvia Guglietta**[1], **John D. Huck**[3], **Catherine Mills**[1], **Anqi Li**[2], **Saleh Rachidi**[1], **Carsten Krieg**[1], **Mark P. Rubinstein**[1,4], **Daniel T. Gewirth**[3], **Shaoli Sun**[5], **Michael B. Lilly**[6], **Amy H. Wahlquist**[7], **David P. Carbone**[2,8], **Yiping Yang**[2,9], **Bei Liu**[1], **Zihai Li**[1,2,8,*]

[1]Department of Microbiology and Immunology, Hollings Cancer Center, Medical University of South Carolina, Charleston, SC 29425, USA.

[2]Pelotonia Institute for Immuno-Oncology, The James Comprehensive Cancer Center, The Ohio State University, Columbus, OH 43210, USA.

[3]Hauptman Woodward Medical Research Institute, Buffalo, NY 14203, USA.

[4]Department of Surgery, Medical University of South Carolina, Charleston, SC 29425, USA.

[5]Department of Pathology and Laboratory Medicine, Medical University of South Carolina, Charleston, SC 29425, USA.

[6]Hollings Cancer Center, Medical University of South Carolina, Charleston, SC 29425, USA.

[7]Department of Public Health Sciences, Medical University of South Carolina, Charleston, SC 29425, USA.

[8]Division of Medical Oncology, The Ohio State University, Columbus, OH 43210, USA.

[9]Division of Hematology, Department of Medicine, The Ohio State University, Columbus, OH 43210, USA.

Abstract

Cancer-associated thrombocytosis and high concentrations of circulating transforming growth factor–β1 (TGF-β1) are frequently observed in patients with progressive cancers. Using genetic and pharmacological approaches, we show a direct link between thrombin catalytic activity and release of mature TGF-β1 from platelets. We found that thrombin cleaves glycoprotein A repetitions predominant (GARP), a cell surface docking receptor for latent TGF-β1 (LTGF-β1) on

*Corresponding author. zihai.li@osumc.edu.

Author contributions: A.M., B.X.W., S.G., J.D.H., C.M., B.R., A.L., C.K., and S.S. performed the experiments. All authors participated in designing various parts of the study and in discussion and interpretation of the results. A.M., B.R., and Z.L. wrote the manuscript with input from all authors. Z.L. supervised the study.

Competing interests: Consulting: Alphamab and Henlius Biotech (Z.L.). Sponsored research agreement: Bristol-Myers Squibb (Z.L. and B.X.W.). Part of the work described in the study was included in a pending patent application (PCT/US2017/025037, Methods for treatment and diagnosis of cancer by targeting GARP and for providing effective immunotherapy alone or in combination, Z.L.). All other authors declare that they have no competing interests.

Data and materials availability: All data associated with this study are present in the paper or the Supplementary Materials.

SUPPLEMENTARY MATERIALS

stm.sciencemag.org/cgi/content/full/12/525/eaay4860/DC1

platelets, resulting in liberation of active TGF-β1 from the GARP–LTGF-β1 complex. Furthermore, systemic inhibition of thrombin obliterates TGF-β1 maturation in platelet releasate and rewires the tumor microenvironment toward favorable antitumor immunity, which translates into efficient cancer control either alone or in combination with programmed cell death 1–based immune checkpoint blockade therapy. Last, we demonstrate that soluble GARP and GARP–LTGF-β1 complex are present in the circulation of patients with cancer. Together, our data reveal a mechanism of cancer immune evasion that involves thrombin-mediated GARP cleavage and the subsequent TGF-β1 release from platelets. We propose that blockade of GARP cleavage is a valuable therapeutic strategy to overcome cancer's resistance to immunotherapy.

INTRODUCTION

Transforming growth factor–β1 (TGF-β1) is one of the major causes for immune checkpoint therapy failure. This is evidenced by multiple studies, indicating that inhibition of the active form of TGF-β1 enhances cancer immunotherapy (1, 2). Therefore, effective targeting of TGF-β1 maturation or function promises to open additional avenues for cancer therapy.

TGF-β1 is an immunosuppressive cytokine that plays important roles in oncogenesis (3–5). Specifically, TGF-β1 modulates the tumor microenvironment by favoring the cancer cells' evasion of immunosurveillance, tempering both the antitumor innate and adaptive immunity (6). With regard to the adaptive antitumor immunity, TGF-β1 inhibits both clonal expansion and cytotoxicity of $CD8^+$ cytotoxic T cells (7) and induces the expression of Foxp3 in $CD4^+$ T cells, therefore conferring a regulatory and immunosuppressive phenotype on these cells (8). In addition, TGF-β1 promotes immune exclusion from tumors by creating a collagen and fibroblast barrier that shields tumors from immune infiltration (9, 10). Consistent with this notion, intense TGF-β1 expression positively correlates with cancer progression and metastasis in several tumor types such as breast carcinoma, prostate cancer, colorectal cancer, and many more (11, 12).

TGF-β1 production and activation consist of multiple tightly regulated steps: First, TGF-β1 is synthesized and targeted into the secretory pathway as inactive homodimeric pre-pro–TGF-β1. After removal of the signal peptide and cleavage by furin-type proteases in the Golgi apparatus, pro–TGF-β1 assembles into the small latent TGF-β1 (LTGF-β1) complex, formed by disulfide bond–linked mature TGF-β1 wrapped around tightly by latency-associated peptide (LAP) in a straitjacket fashion (13–15). Last, the release of the biologically active TGF-β1 requires the proteolytic or mechanical separation of the mature form of TGF-β1 from the LAP. Multiple mechanisms have been evoked to be at play at this critical step, in which cell surface proteins such as integrins and glycoprotein A repetitions predominant (GARP) are the main orchestrators (16–18).

GARP is a cell surface docking receptor for LTGF-β1 and is mostly expressed on induced regulatory T cells (T_{regs}), platelets, and cancer cells (19–21). A growing body of work indicates that GARP plays a critical role in the maturation of LTGF-β1, which results in cancer progression and peripheral tolerance (17, 22–24). We previously demonstrated that release of active TGF-β1 from platelets depends on GARP–LTGF-β1 complex and that platelet-derived active TGF-β1 jeopardizes the antitumor T cell function (25). However, the

molecular mechanism that is responsible for the release of mature TGF-β1 from the GARP–LTGF-β1 complex remains incompletely understood. In addition, although a soluble form of GARP–LTGF-β1 is present in human plasma (26), it is currently unclear how it is generated and whether the release of GARP regulates LTGF-β1 activation.

Here, we describe a process in which the serine protease thrombin mediates the release of active TGF-β1 by cleaving surface GARP on platelets. Furthermore, we demonstrate that pharmacological inhibitors of GARP cleavage abrogate platelet LTGF-β1 activation and increase the therapeutic efficacy of programmed cell death 1 (PD-1) blockade against multiple preclinical cancer models.

RESULTS

Serine protease thrombin cleaves surface GARP and mediates the activation of TGF-β1 from the GARP–LTGF-β1 complex

We previously demonstrated that an endoplasmic reticulum molecular chaperone glycoprotein 96 (gp96) is critical for cell surface expression of GARP and the membrane-bound LTGF-β1 (27). To further investigate the role of gp96 in the maturation of GARP, we stably expressed GARP in wild-type (WT) and gp96 null mouse pre–B leukemic cell line 70Z/3. Total cell lysate analysis by immune-blot revealed the presence of three mouse GARP bands: full-length protein (72 kDa) expressed in both WT and gp96-deficient cells and two smaller forms of GARP of 40.7 and 29.5 kDa in WT but not gp96 null cells (Fig. 1A). The formation of smaller fragments of GARP only in the presence of gp96 supported the idea that GARP might be shed at the cell surface and released into the extracellular milieu. To address this possibility, we analyzed the presence of GARP in both cell lysate and conditioned medium of WT GARP-expressing cells. We observed that the 29.5-kDa fragment was abundantly present in the conditioned medium (Fig. 1B). Mass spectrometry analysis confirmed that this fragment belongs to part of the N^{+}-terminal domain of GARP (Fig. 1C). We also expressed human GARP in human embryonic kidney (HEK) 293 cells and observed the presence of full-length GARP, as well as a smaller fragment of 42.7-kDa molecule in the cell lysate and the supernatant (Fig. 2A). We next examined GARP processing in primary human platelet lysates and releasates biochemically. In the total cell lysate of platelets, besides the expected 72-kDa band (whole protein), a GARP fragment of 42.7 kDa was detectable. We also readily observed the presence of a 21.4-kDa fragment of GARP in the human platelet releasate generated by incubating platelets with thrombin (Fig. 2B).

We next focused on defining the protease that is responsible for GARP cleavage. GARP amino acid sequence analysis using the ExPASy portal led us to focus on thrombin for two main reasons: First, there are two predicted thrombin cleavage sites in both mouse and human GARP. If thrombin-mediated GARP cleavage occurs, then two GARP fragments will be generated, corresponding to the precise sizes that we have seen (fig. S1A). Second, one of the predicted thrombin binding sites is phylogenetically conserved (fig. S1B).

To prove that thrombin is indeed responsible for GARP cleavage, we mutated the two predicted Pro-Arg (PR) thrombin binding sites of human GARP to Ala-Ala to generate two

single mutants and one double mutant: GARP^{P198A,R199A} (Mut 1), GARP^{P266A,R267A} (Mut 2), and GARP^{P198A,R199A,P266A,R267A} (2xMut). Both Mut 1 and Mut 2 could be expressed abundantly on the cell surface, but the double mutant failed to do so (fig. S1C). All mutations substantially reduced GARP cleavage (Fig. 2C). To further confirm our findings, recombinant human GARP was digested in the presence of either active thrombin or a variant of the same enzyme with a blocked active site. We observed a dose-dependent cleavage of GARP by active thrombin to generate the two GARP fragments (40 and 22 kDa), as we have observed in the activated human platelets (Fig. 2D). A 3.1-Å resolution crystal structure of the GARP–LTGF-β1 complex has recently been resolved (28). In agreement with our data showing that GARP can be cleaved by thrombin, both thrombin cleavage sites on GARP are located on the opposite face of the bound LTGF-β1 and are surface exposed. To determine whether a ternary complex of thrombin-GARP–LTGF-β1 is structurally plausible, we docked an existing crystal structure of thrombin onto the GARP–LTGF-β1 complex using the ClusPro web server (Fig. 2E) (29). Twenty-nine putative models of the ternary complex were generated. Twenty-two of 29 models docked thrombin onto the concave surface of GARP opposite LTGF-β1, supporting that thrombin is able to cleave the LTGF-β1–bound form of GARP. GARP expression facilitates processing of pro–TGF-β1 and secretion of LTGF-β1 (27, 30). To study the role of GARP cleavage in LTGF-β1 activation and/or release, we enforced TGF-β1 expression in HEK293 cells that also coexpress either WT or human GARP mutants or no GARP as control. We first checked whether mutated GARP affected TGF-β1 expression or surface GARP-LAP binding. We found that TGF-β1 expression was not affected by GARP mutations (fig. S2A), and the GARP single mutant (but not double mutant) still retained the ability to bind to LTGF-β1 (fig. S2B). As previously described (30), we found that GARP associates with pro–TGF-β1 to form a large 160-kDa complex (Fig. 2F). To look at the function of thrombin in releasing mature TGF-β1 extracellularly from the GARP–LTGF-β1 complex, we analyzed the conditioned media of GARP mutants by Western blot. We observed a complete reduction of the release of latent and active TGF-β1 when GARP cleavage was impaired, indicating that GARP proteolytic cleavage is a prerequisite for the release of mature TGF-β1 (Fig. 2G). Moreover, the release of pro–TGF-β1–GARP complex was markedly reduced when surface GARP was not properly cleaved by thrombin (Fig. 2, G and H). Overall, these results unveil a mechanism of TGF-β1 activation triggered by the interaction of GARP with the serine protease thrombin and the subsequent cleavage of surface GARP.

Human and mouse GARP share almost 80% homology at the amino acid level with 100% conservation at one of the two thrombin binding sites (fig. S1). We confirmed that thrombin is also responsible for cleaving mouse GARP by a series of experiments. First, mouse GARP stably expressed on the cell surface of pre–B cells can be cleaved by thrombin in a dose-dependent manner to generate two predicted 44- and 29-kDa fragments (Fig. 3A). Second, we performed a competition assay using a 50-amino acid–long peptide from GARP named T250 that contains two thrombin binding sites (Fig. 3B). We found that T250 can partially block thrombin-mediated GA0RP cleavage (Fig. 3C). Third, similar to human GARP, a molecular modeling of the mouse GARP–LTGF-β1 complex demonstrated that both of the thrombin sites on mouse GARP are also surface exposed and therefore accessible to thrombin for cleavage (Fig. 3D). Last, we confirmed the importance of two thrombin

binding sites using site-directed mutagenesis. The three mouse GARP mutants we generated are: $GARP^{P267A,R268A}$ (Mut 1), $GARP^{P286A,R287A}$ (Mut 2), and $GARP^{P267A,R268A,P286A,R287A}$ (2xMut). All three mutants can be stably expressed on the cell surface, suggesting proper folding and trafficking of these mutants (Fig. 3E). Whereas mutation of each thrombin binding site alone reduced GARP cleavage, mutation of both sites abrogated GARP cleavage (Fig. 3F).

Proteolysis of platelet GARP mediates systemic LTGF-β1 activation and tumor progression

We previously demonstrated that platelet GARP is essential for active TGF-β1 release in platelet releasate (25). In addition, it is known that platelets create their own pool of thrombin by supporting the in situ activation of prothrombin to fully active thrombin (31, 32). On the basis of this evidence, we hypothesized that platelet thrombin is responsible for cleaving surface platelet GARP to release mature TGF-β1 from the surface GARP–LTGF-β1 complex. To test this hypothesis, we isolated platelets from WT and platelet-specific GARP knockout (plt-GARP KO) mice and activated them in the presence or absence of thrombin. We found that platelet GARP undergoes the same cleavage pattern observed in HEK293 cells (Fig. 4A) and, more importantly, we observed that thrombin activation enhanced mature TGF-β1 release only from WT but not GARP KO platelets, as detected by Western blot and enzyme-linked immunosorbent assay (ELISA) (Fig. 4, B and C). Given that TGF-β1 is the main suppressive molecule within platelet releasate for T cell proliferation (25), we next performed an in vitro T cell activation assay using mouse splenocytes in the presence of WT or GARP KO platelet releasate. We found that, unlike WT platelet releasate, the releasate from GARP KO platelets had reduced activity in blocking T cell proliferation (Fig. 4D). Furthermore, we found that T250 peptide can block the production of mature TGF-β1 from platelet releasate (Fig. 4E) yet without affecting platelets' activation status (Fig. 4F). This work collectively demonstrated that GARP cleavage is a prerequisite for platelet TGF-β1 maturation.

We recently reported that platelet GARP enhances tumor growth by activating LTGF-β1 systemically and in the tumor microenvironment (25). We next studied the role of thrombin-mediated GARP cleavage in generating active TGF-β1 in vivo by using direct thrombin inhibitor dabigatran etexilate. We hypothesized that by blocking thrombin-mediated platelet GARP cleavage, dabigatran etexilate would be able to reduce active TGF-β1 systemically and thereby diminish tumor growth. First, to exclude that any effect exerted by dabigatran etexilate was a consequence of a general platelet dysfunction, we evaluated the platelet number and activation in mice treated with dabigatran etexilate. Consistent with a previous study (33), platelet reactivity as measured by GARP and P-selectin expression was not altered by dabigatran etexilate and neither was the platelet number (Fig. 5A). However, systemic thrombin inhibition markedly reduced the active, but not total TGF-β1 released by platelets during the formation of blood clots, as demonstrated by serum TGF-β1 (Fig. 5B). To further uncouple the systemic platelet inactivation from the specific thrombin inhibition, we compared serum active TGF-β1 in mice treated with dabigatran etexilate versus other antiplatelet agents, clopidogrel and aspirin. We observed that only by specifically blocking thrombin proteolytic activity was it possible to achieve a potent reduction of active TGF-β1 released from blood clots (Fig. 5C). Next, to conclusively demonstrate that thrombin is

acting on the platelet GARP–LTGF-β1 axis, WT and plt-GARP KO mice were injected subcutaneously with MC38 colon carcinoma cells, followed by treatment with dabigatran etexilate. As reported previously, dabigatran etexilate alone had antitumor efficacy in this model (4, 34); however, this property was completely lost in plt-GARP KO mice (Fig. 5D). The reduction in the serum active TGF-β1 observed in WT mice was not observed in the absence of platelet GARP (Fig. 5E), indicating that thrombin mediates the activation of TGF-β1 primarily by acting on platelet GARP. We also quantified the cell surface GARP on the platelets in WT mice before and after treatment with dabigatran etexilate. We reasoned that if GARP cleavage is mediated by thrombin, then administration of thrombin inhibitors should result in elevation of surface GARP on platelets. We found that there was a small but significant increase in the cell surface GARP ($P < 0.01$) and LAP ($P < 0.001$) on platelets in mice that were treated with dabigatran daily for 5 days compared with untreated mice (Fig. 5, F and G).

Cleavage of platelet GARP supports protumorigenic and immune-evasive tumor microenvironment

We showed that thrombin inhibition by dabigatran etexilate reduces the GARP-dependent production of TGF-β1 from platelets and prevents tumor progression. On the basis of these findings and the known roles of TGF-β1 in immune suppression and oncogenesis (35), we next investigated the effect of thrombin blockade on the tumor microenvironment. To this end, we subcutaneously injected WT C57BL/6 mice with MC38 colon carcinoma cells and treated them with dabigatran etexilate or left them untreated. Histological analysis of tumor sections revealed that dabigatran etexilate blocks TGF-β1 deposition in both the tumor bed and the stroma (Fig. 6A). In line with this observation, indicators of TGF-β1 signaling, including deposition of collagen and smooth muscle actin (SMA), were reduced in mice treated with dabigatran etexilate (Fig. 6A). Dabigatran etexilate did not affect platelet infiltration into the tumor, which was observed primarily in the proximity of blood vessels (Fig. 6A). To understand how and whether treatment with dabigatran etexilate affects the immune response at the tumor site, we performed an unbiased multiparameter analysis of the immune infiltrates in the draining lymph nodes and tumors by using mass cytometry. We found that dabigatran etexilate treatment greatly rewired the tumor microenvironment by increasing tumor-infiltrating $CD8^+$ T cells and innate natural killer (NK) cells and neutrophils (Fig. 6, B and C). GARP expression on T_{regs} is an indicator of an active and strong immunosuppressive phenotype (36), and for this reason, we evaluated GARP expression on intratumoral T_{regs} by flow cytometry. T_{regs} isolated from MC38 tumors of mice treated with dabigatran etexilate showed less surface GARP expression, indicating that TGF-β1 derived from cleavage of platelet GARP enhances the suppressive ability of tumor T_{regs} (Fig. 6, D and E). The frequency of functional $CD8^+$ T cells [interferon-γ (IFNγ) producing] was not significantly different ($P = 0.05$) in the dabigatran group (Fig. 6F). Coupled with the functional difference in tumor rejection and the mass cytometry data, these data suggested that dabigatran treatment indeed rewired the tumor microenvironment into an immunologically favorable one.

Blocking platelet GARP cleavage enhances efficacy of immune checkpoint blockade therapy in preclinical cancer models

Intratumoral and systemic TGF-β1 constitutes a major hindrance for immune checkpoint inhibitors (2, 37). We hypothesized that dabigatran etexilate could overcome anti–PD-1 resistance in cancer therapy because of its ability to reduce TGF-β1. We used two preclinical tumor models to test our hypothesis: MC38 colorectal cancer and EMT-6 triple-negative breast cancer. In both preclinical models, PD-1 and antithrombin treatment were started at the same time, when the tumors reached a size of about 30 mm^2. Single therapies reduced MC38 tumor growth, but mice treated with the combination of anti–PD-1 and dabigatran etexilate had the strongest treatment response, with five of the seven mice showing stable disease control and three achieving total tumor regression (Fig. 7, A and B). In addition, only mice treated with dabigatran etexilate, either alone or in combination with PD-1 antibody, experienced a marked drop in the serum active TGF-β1 (Fig. 7C). Similar effects were observed in the EMT-6 tumor model, where combined antithrombin therapy and PD-1 antibody blockade showed much better tumor control and enhanced survival compared to either agent alone (Fig. 7, D and E). The success of the combination therapy was highlighted by the reduction in metastatic tumor burden observed in the lungs of EMT-6–bearing BALB/c mice (Fig. 7F), likely due to the improved checkpoint blockade therapy after reduction of active TGF-β1 (Fig. 7G).

Soluble GARP and GARP–LTGF-β1 complex are present in patients with cancer

Increased thrombin activity, thrombocytosis, and platelet activation are frequently associated with human malignancy (38, 39). Our present study demonstrated that thrombin cleaves GARP, resulting in release of soluble GARP (sGARP)–LTGF-β1 complex and liberation of active TGF-β1. We next examined whether sGARP is present in patients with cancer. We examined patients with prostate cancer because a high concentration of plasma TGF-β1 has been reported to be a strong indicator of poor clinical outcome in this disease (40). We surmised that plasma derived from patients with prostate cancer may have a high concentration of sGARP and sGARP–LTGF-β1 complex. We found that the concentration of sGARP in the plasma of patients with prostate cancer (325.6 pg/ml ± 37.88, $n = 47$) was higher than that of healthy individuals (143.2 pg/ml ± 30.82, $n = 7$) (Fig. 8A). Using the upper limit of sGARP concentration as a cutoff (150 pg/ml), we found that 71.5% of patients above the cutoff had concentrations of prostate-specific antigen (PSA) higher than 10 ng/ml, whereas less than 33.3% of patients with low sGARP had higher PSA ($P < 0.0001$). Similarly, 57% patients with high sGARP had metastasis as opposed to 33.3% with low sGARP ($P < 0.001$) (Fig. 8B).

In addition, we developed a sandwich ELISA to evaluate the concentration of sGARP in complex with LTGF-β1 (sGARP–LTGF-β1). We found that the concentration of the complex was higher in plasma collected from patients with prostate cancer compared to healthy controls ($P = 0.0305$) (Fig. 8C). Together, our findings indicate the presence of both sGARP and GARP–LTGF-β1 complex in the plasma of patients with cancer.

DISCUSSION

The role of platelets in promoting cancer invasion has been previously observed (41–43). As a chronic unhealed wound, cancer constantly activates the coagulation pathway that culminates with the generation of high concentration of thrombin locally, resulting in chronic platelet activation (44). We previously demonstrated that TGF-β1 is the most abundant protumorigenic and immune suppressive cytokine released by active platelets. We also showed that platelet-intrinsic GARP plays a dominant role in activating LTGF-β1 (25). Here, we describe a thrombin-dependent mechanism of TGF-β1 maturation from the platelet GARP–LTGF-β1 complex that involves cleavage of GARP on the plasma membrane. This work suggests an intricate linkage between coagulation and platelet activation, contributing to subsequent immune evasion and cancer progression.

We demonstrated that thrombin is responsible for cleaving both human and mouse GARP to generate a soluble N-terminal fragment that is abundantly released into the extracellular milieu. By site-directed mutagenesis and biochemical analysis, we also showed that GARP cleavage regulates the formation and release of both active TGF-β1 and sGARP–LTGF-β1 complex. Moreover, we found that the thrombin-platelet GARP–LTGF-β1 axis is a relevant pathway for cancer immunotherapy, because (i) direct thrombin inhibitor blunted release of active TGF-β1 systemically; (ii) inhibition of thrombin caused rewiring of the immune response in the tumor microenvironment; (iii) the antitumor effect of thrombin is dependent on platelet-intrinsic GARP; and (iv) direct thrombin inhibitor can enhance the preclinical responsiveness of cancers to PD-1 immune checkpoint blockade.

Our study does not exclude other proteases and/or integrins in LTGF-β1 activation. GARP–LTGF-β1 complex can be expressed on many other cell types such as T_{regs} (19), cancer cells (20), and B lymphocytes (23), where thrombin might not be the key player in TGF-β1 maturation. For example, it has been demonstrated that αVβ8 integrin regulates LTGF-β1 maturation from the GARP–LTGF-β1 complex on T_{regs} (45), as well as on HEK293 cells (17). The association between GARP–LTGF-β1 complex and integrins does not disrupt the ring-like structure of LTGF-β1, suggesting that integrins interaction is necessary but not sufficient for secretion of mature TGF-β1 (17). This may indicate that, similar to soluble LTGF-β1, extra forces are required for the removal of the “straightjacket” elements of LAP from the GARP–LTGF-β1 complex (16).

Consistent with the genetic studies, pharmacological inhibition of thrombin was effective in reducing active but not total TGF-β1 in the serum. In this study, we used dabigatran etexilate, a competitive and reversible direct thrombin inhibitor approved for venous thrombolytic events (46). Dabigatran etexilate blocks thrombin-induced platelet aggregation, although it has no effect on platelet activation induced by other agonists such as adenosine 5′-diphosphate and collagen (47). The antitumor properties of dabigatran etexilate in preclinical models of breast and pancreatic cancer were previously reported without clear mechanistic explanation (34, 48). Here, we report the existence of a platelet-specific thrombin-GARP–TGF-β1 axis, which contributes to tumor progression by enhancing the accumulation of platelet-derived TGF-β1 in the tumor microenvironment. By up-regulating collagen (49), TGF-β1 confers a selective advantage to the growing tumor by shaping a

protumorigenic immune landscape where the infiltration and the tumoricidal activity of NK cells (50), neutrophils (51), macrophages, and cytotoxic T lymphocytes (52) are restrained. We saw profound changes of these immune subsets in the tumors in mice receiving dabigatran etexilate treatment. Compared to systemic TGF-β1 inhibition, thrombin blockade has the advantage of neutralizing the activation of platelet-derived TGF-β1 in the blood clots occurring around the peritumoral area. Furthermore, specific thrombin inhibition also has the potential to reduce cancer cell migration and metastasis, as shown by the metastatic breast cancer model in the current study. Our work therefore should inspire future efforts to develop inhibitors to block GARP cleavage specifically for cancer immunotherapy, especially because the combination of immune checkpoint blockade and TGF-β1–targeted therapy has been shown to overcome immune resistance (2, 37, 53, 54).

Our clinical data indicate that sGARP may be a potential biomarker for prostate cancer. Prostate cancer is the most commonly diagnosed cancer among elderly men and the second leading cause of cancer death in Western countries (55). Circulating PSA is routinely screened as a prognostic and diagnostic tool, yet several limitations exist regarding its specificity and effectiveness in prediction of clinical outcomes (56, 57). Our study showed that higher concentrations of sGARP in the plasma are more commonly found in patients with advanced stage of prostate cancer and worse clinical outcome. We also found that sGARP is present in normal subjects, indicating perhaps other still yet to be defined homeostatic roles of GARP cleavage in immune tolerance and other biological processes. However, the human relevance of our study is limited due to lack of comorbidity information and missing of detailed clinical outcome of study subjects. Further studies are warranted to define the utility of sGARP as a marker for cancer and other diseases in general, as well as, more specifically, for patients undergoing immunotherapy including immune checkpoint blockers.

In conclusion, our study has uncovered thrombin-mediated GARP cleavage as a mechanism for immune tolerance and cancer progression via the activation of LTGF-β1 from platelets. Targeting GARP cleavage has the potential to overcome primary and secondary resistance of cancer to immunotherapy.

MATERIALS AND METHODS

Study design

This study investigated the mechanism of LTGF-β1 activation from the GARP–LTGF-β1 complex on multiple cell types and the potential of blocking GARP cleavage for cancer immunotherapy. This was accomplished using several complementary approaches including molecular biology, mouse genetics, biochemistry, and immunology. In vitro experiments were typically carried out using >3 biological repeats and in >3 independent experiments. Syngeneic mouse tumor models were adopted for in vivo experiments, using >5 animals per condition, which were conducted in >3 independent experiments. For in vivo experiments, mice were randomized into each group. Tumor growth and tumor-infiltrating lymphocytes were measured without blinding, but pathological evaluations were performed by a board-certified pathologist (S.S.) without knowledge of specific intervention or mouse genotypes. The presence of sGARP in the sera of patients and normal subjects was verified using

archived plasma or serum samples with the investigators blinded to patient information. Primary data are reported in data file S1.

Patients and clinical samples

The aim of this study was to test the diagnostic and prognostic relevance of sGARP concentration in plasma from patients with cancer. This study included patients with prostate cancer prospectively enrolled at Medical University of South Carolina, SC, USA, under an approved institutional review board protocol number CTO 101814. Informed consent was obtained from all patients. Blood samples were collected before starting treatment, and plasma samples were obtained at the time of diagnosis.

Cell lines

Pre–B cell line (70Z/3) was a gift from B. Seed (58). MC38 tumor cells were obtained from M. Rubinstein (Medical University of South Carolina). EMT-6 and HEK293FT cell lines were purchased from American Type Culture Collection. HEK293FT and MC38 cells were cultured in Dulbecco's modified Eagle's medium (DMEM) with 10% fetal bovine serum, 100 U/ml penicillin, and streptomycin (100 μg/ml) in a humidified atmosphere of 95% air and 5% CO_2 at 37°C. Pre–B cells were cultured in RPMI 1640 medium with 10% fetal bovine serum, 100 U/ml penicillin, streptomycin (100 μg/ml), and 1% β-mercaptoethanol in a humidified atmosphere of 95% air and 5% CO_2 at 37°C. EMT-6 cells were cultured in Waymouth's MB 752/1 medium with 2 mM L-glutamine, 10% fetal bovine serum, 100 U/ml penicillin, and streptomycin (100 μg/ml) in a humidified atmosphere of 95% air and 5% CO_2 at 37°C. Cancer cells were authenticated by gene expression analysis, in vivo growth, and histology. All the lines were monitored for pathogens, and we routinely performed mycoplasma analysis on the lines.

Mice

C57BL/6 WT and BALB/c mice were purchased from The Jackson Laboratory. Platelet-specific GARP KO mouse was generated by crossing *Lrrc32*$^{flox/flox}$ mice (59) with *Pf4-Cre* mice (60). All animal experiments were conducted under protocols approved by the Institutional Animal Care and Use Committee at Medical University of South Carolina and The Ohio State University.

Generation of GARP-expression vectors and site-directed mutagenesis

Human and mouse GARP were amplified by polymerase chain reaction and subcloned between the BglII and HpaI sites in a MigR1 retroviral vector as previously described (61). For site-directed mutagenesis, PR at 267 to 268 and 286 to 287 amino acid positions were both mutated to alanine-alanine using the QuikChange II XL Site-Directed Mutagenesis Kit (Stratagene). For murine GARP, we used the following primers: 267–268 point mutation, GGCCGTGTTCGCGGCACTCATCTACC (forward) and GGTAGATGAGTGCCGCGAACACGGCC (reverse); 286–287 point mutation, GCGGGGCTGGCCGCAGGCAGTGAGG (forward) and CTCACTGCCTGCGGCCAGCCCCGCA (reverse).

For human GARP, we used the following primers: 198–199 point mutation, CCTTCGAGGGTCTGGCAGCACTGACCCATCTC (forward) and GAGATGGGTCAGTGCTGCCAGACCCTCGAAGG (reverse); 266–267 point mutation, ACCTGGCCGCGCTCGCAGCACTCATCTACCTGAA (forward) and TTCAGGTAGATGAGTGCTGCGAGCGCGGCCAGGT (reverse). All constructs were subcloned into MigR1 retroviral vector for retrovirus production as previously reported (61). The efficiency of mutagenesis was assessed by DNA sequencing, Western blotting, and flow cytometry analysis.

Flow cytometry

For flow cytometry staining, cells were washed twice in fluorescence-activated cell sorting (FACS) buffer, and FcR blocking was applied 10 min at 4°C. Live/dead staining was performed for 10 min at 4°C with Fixable Viability Dye (Affymetrix) before staining with the surface antibody mix (indicated in each figure) for 30 min at 4°C in FACS buffer. For intracellular staining, Foxp3/Transcription Factor Staining Buffer Set (Affymetrix) was used according to the manufacturer's protocol. Samples were analyzed immediately on BD FACSDiva, and data analysis was performed using FlowJo Software (Tree Star). Antibodies against human GARP (7B11 BioLegend), human LAP (eBioscience TW4–2F8), mouse GARP (eBioscience YGIC86), and mouse P-selectin (eBioscience Psel.KO2.3) were used.

Mass cytometry acquisition and analysis

Mass cytometry single-cell analysis was performed as previously described (24). For single-cell preparation from tumors, tumors were minced into small pieces with a blade, resuspended in DMEM with 10% fetal calf serum (FCS) plus 1% collagenase D, digested in a water bath at 37°C for 30 min, passed through a 40-μm cell strainer, and stained following the published protocol (62). Briefly, to reduce intersample staining variability, minimize sample handling time, and reduce antibody consumption, we used live cell barcoding approach. Therefore, isothiocyanobenzyl-EDTA (p-SCN-EDTA; Dojindo) was loaded with four different palladium isotopes (^{104}Pd, ^{105}Pd, ^{106}Pd, and ^{108}Pd) and two indium isotopes (^{113}I and ^{115}I) to label anti-mouse CD45.2 (BioLegend) as barcoding reagents. Draining lymph node cells or tumors were labeled with metal-tagged CD45.2 antibodies for 15 min in cell staining medium (CSM) [phosphate-buffered saline (PBS), 2% FCS, and 1 mM EDTA] on ice. Samples were washed twice in CSM and combined into a single reaction vessel for further staining steps. After live cell barcoding, the combined sample was centrifuged, the supernatant was aspirated, and cells were resuspended in 300 μl of antibodies in CSM. Cells were stained with antibodies for 20 min at 4°C. Dead cells were excluded by adding 1 ml of 2.5 μM cisplatin (Sigma-Aldrich) in PBS at the end of the staining period and incubating for 2 min at room temperature. Afterward, the sample was washed once in PBS supplemented with 5% FCS. Last, cells were incubated overnight with 250 nM iridium intercalator (Fluidigm) to label cellular DNA. Subsequently, cells were washed with PBS.

Samples were acquired on a CyTOF-Helios mass cytometer (Fluidigm). Quality control and tuning processes were performed on a daily basis before acquisition. Before downstream analysis, data acquired by mass cytometry were normalized using the standalone MATLAB normalizer (version 2013b), and marker expression was controlled in FlowJo (version

10.1r5). Next, live cells were exported by manual gating on Event_length, DNA (^{191}Ir and ^{193}Ir), and live cells (^{195}Pt) using FlowJo software (Tree Star), and individual samples were debarcoded using Boolean gating. We combined elements of an earlier workflow (63) with visualizations from the CATALYST package (64) and applied the FlowSOM algorithm (65) for clustering cells into putative subpopulations.

Immunohistochemistry

Fixed tissue was incubated overnight in 70% ethanol before paraffin embedding and then cut with a cryotome for hematoxylin and eosin and immunohistochemistry staining. Antigen retrieval was performed in tris-EDTA buffer (pH 9). To minimize nonspecific staining, sections were incubated with normal goat serum for 20 min at room temperature, followed by incubation with primary anti–α-SMA1 antibody (Sigma A2547), anti–LTGF-β1 (MyBioSource MBS856490), and anti-CD61 antibody (Cell Signaling 13166) overnight at 4°C. Staining with secondary antibodies (Vectastain ABC Kit) was then performed before development using dabigatran substrate (Vector Laboratories SK-4100). For Masson's trichrome staining of collagen, formalin-fixed paraffin-embedded sections were deparaffinized using xylene and hydrated with descending alcohol series (100, 90, 70, and 60%). Thereafter, sections were stained according to the manufacturer's protocols (Polysciences Inc., 25088). Scoring was performed by the study pathologist (S.S.) without knowledge of the sample identification: intensity scale (0 to 5: 0, no signal; 1, borderline; 2, weakly positive; 3, positive; 4, strongly positive; 5, the brightest signal) and distribution of the staining (percentage in the histology field).

Protein extraction, immunoprecipitation, and Western blot analysis

Adherent cells were harvested by trypsin-EDTA, washed in PBS, and lysed on ice in radioimmunoprecipitation assay lysis buffer in the presence of a protease inhibitor cocktail (Sigma-Aldrich). Nuclear-free protein lysate was quantified by Bradford assay (Bio-Rad), and an equal amount of lysate was analyzed by SDS–polyacrylamide gel electrophoresis (PAGE) and Western blot under reducing and nonreducing conditions using anti-mouse GARP (AF6229; R&D System) and anti–TGF-β1 (A75–2 555052; BD Pharmingen).

Activation of platelets and preparation of releasate from activated platelets

Platelet-specific GARP KO and control mice were anesthetized, and blood was withdrawn into a 5-ml tube containing another 0.5 ml of acid citrate dextrose buffer [39 mM citric acid, 75 mM sodium citrate, 135 mM dextrose, and prostaglandin E1 (1 μg/ml) (pH 7.4)]. Samples were centrifuged for 10 min at 100*g*, with no brake, and the upper layer of platelet-rich plasma was collected. Platelets were washed twice with citrate washing buffer [128 mM NaCl, 11 mM glucose, 7.5 mM Na_2HPO_4, 4.8 mM sodium citrate, 4.3 mM NaH_2PO_4, 2.4 mM citric acid, 0.35% bovine serum albumin, and prostaglandin E1 (50 ng/ml) (pH 6.5)], then resuspended in RPMI 1640, enumerated by a blood cell counter, and diluted to a final concentration of 1×10^8/ml. Purified platelets were incubated with or without mouse thrombin (Enzyme Research Laboratories) for 1 hour at 37°C at 125 rpm. Stimulated platelets were sedimented by centrifugation for 15 min at 3200*g*, and the supernatant was collected and stored at −80°C.

Soluble TGF-β1 ELISA

Mouse blood was collected through submandibular bleeding in Eppendorf tubes, left to coagulate for 1 hour at room temperature, and centrifuged at 5000 rpm for 15 min. Human blood (10 ml) was collected in tubes containing lithium heparin anticoagulant. The blood was then centrifuged at 1000*g* for 7 min. The plasma was then removed, aliquoted, and stored at −80°C. Capture ELISA for TGF-β1 was performed according to manufacturer instructions (BioLegend). Active TGF-β1 was measured with no additional manipulation. Total TGF-β1 was measured after acidic activation using 1 M HCl for 10 min at room temperature and neutralization with 1.2 NaOH and 1 M Hepes. Active TGF-β1 and total TGF-β1 were measured using TGF-β1 ELISA kits according to the manufacturer's protocols (BioLegend). The same TGF-β1 ELISA procedure was adopted for platelet releasate.

GARP–TGF-β1 sandwich ELISA

To measure GARP–TGF-β1 complex by ELISA, 96-well plates were coated with TGF-β1 capture antibody according to the manufacturer's instructions (BioLegend). Samples were incubated for 2 hours at room temperature, followed by incubation with the anti-GARP detection antibody developed by our lab for 2 hours.

Thrombin digestion

A total of 1×10^6 GARP-expressing cells and 1 μg of recombinant GARP protein were resuspended in thrombin buffer: 50 mM tris-HCl (pH 8.0), 100 mM NaCl, 2.5 mM $CaCl_2$, and 0.1% β-mercaptoethanol. Cells were digested for 1 hour at room temperature with either mouse or human α-thrombin (Enzyme Research) or with a thrombin mutant that has its active site blocked, α-thrombin–Biotinylated Phe-Pro-Arg-Chloromethylketone (BFPRCK) (Haematologic Technologies).

T-250 peptide

Thrombin cleavage blocking experiment was performed using the following peptide: DLRENKLLHFPDLAVFPRLLIYLNVSNNLIQLPAGLPRGSEDLHAPSEGWSA which was generated at Hangzhou Dangang Biological Technology.

Mass spectrometry

Cell lysate was loaded, and SDS-PAGE was run. Gel was stained with Coomassie blue, and the fragment of interest was subjected to in-gel protease digestion, chromatographic separation and tandem mass spectrometry (MS/MS) analysis of the resulting peptides, and interpretation of MS/MS data using SEQUEST software.

Tumor protection experiments

For MC38 tumor model, WT or plt-GARP KO mice were injected in the right flank with 1×10^6 MC38 colon cancer cells. For EMT-6 tumor model, female mice were injected with 1×10^5 triple-negative breast cancer cells in the fourth mammary fat pad. For the antithrombin therapy, mice were gavaged daily with 3 mg per mouse of dabigatran etexilate (Boehringer Ingelheim) dissolved in water. A dose of 200 μg per mouse of anti-mouse PD-1 blocking

antibody (BioXCell) was intraperitoneally administered every 3 days. Tumor area was measured every 3 days with digital vernier caliper.

Structural modeling

GARP amino acidic sequence was analyzed for potential protease cleavage sites using the ExPASy portal (https://web.expasy.org/peptide_cutter/). Thrombin docking onto human GARP–LTGF-β1 was performed using the ClusPro server (29). Thrombin [Protein Data Bank (PDB) ID 1A2C; chain H] was used as the ligand input, and GARP/LTGF-β1 (PDB ID 6GFF; chains A, B, C, D, and I) was used as the receptor input. Each of the calculated models was inspected manually using PyMOL. The lowest energy model, in which the active site of thrombin was pointed toward the cleavage sites on GARP, was chosen as the representative model.

To analyze the locations of the thrombin cleavage sites on mouse GARP, a model of the mouse GARP ectodomain (residues 18 to 628) was generated using human GARP from PDB ID 6GFF (human GARP/LTGF-β1/MHGARP8) as a template in SWISS-MODEL (ExPASy) (66). Mouse GARP was then superimposed onto human GARP using PyMOL for analysis.

Statistical analysis

Student's *t* test was used to compare categorical variables such as normal versus cancer or different disease stages or categories. Time to reach the end point was analyzed by Kaplan-Meier curves. Tumor growth curve analysis was performed using two-way analysis of variance (ANOVA). All data are presented as means ± SD except data shown in Fig. 5C (means ± SEM). $P < 0.05$ was considered to be statistically significant. χ^2 test was used to analyze the correlation of high and low serum GARP with percentages of patients with prostate cancer presenting with high PSA1 (higher than 10) and secondary tumors. Adjusted *P* value based on computational framework diffcyt was used for CyTOF data analysis. Original data are provided in data file S1.

Supplementary Material

Refer to Web version on PubMed Central for supplementary material.

Acknowledgments:

We thank the following individuals for sharing reagents used in this work: P. Howe (MUSC), C. Paulos (MUSC), and B. Seed (Harvard). We thank the past and present members of the Li laboratory for stimulating discussions and support during the entire course of the study.

Funding: Research in the Li laboratory is supported by multiple NIH grants (AI077283, CA188419, CA213290, DK105033, and CA186866).

REFERENCES AND NOTES

1. David JM, Dominguez C, McCampbell KK, Gulley JL, Schlom J, Palena C, A novel bifunctional anti-PD-L1/TGF-β Trap fusion protein (M7824) efficiently reverts mesenchymalization of human lung cancer cells. Oncoimmunology 6, e1349589 (2017). [PubMed: 29123964]

2. Ravi R, Noonan KA, Pham V, Bedi R, Zhavoronkov A, Ozerov IV, Makarev E, Artemov AV, Wysocki PT, Mehra R, Nimmagadda S, Marchionni L, Sidransky D, Borrello IM, Izumchenko E, Bedi A, Bifunctional immune checkpoint-targeted antibody-ligand traps that simultaneously disable TGFβ enhance the efficacy of cancer immunotherapy. Nat. Commun 9, 741 (2018). [PubMed: 29467463]
3. Bhowmick NA, Ghiassi M, Bakin A, Aakre M, Lundquist CA, Engel ME, Arteaga CL, Moses HL, Transforming growth factor-β1 mediates epithelial to mesenchymal transdifferentiation through a RhoA-dependent mechanism. Mol. Biol. Cell 12, 27–36 (2001). [PubMed: 11160820]
4. Alexander ET, Minton AR, Hayes CS, Goss A, Van Ryn J, Gilmour SK, Thrombin inhibition and cyclophosphamide synergistically block tumor progression and metastasis. Cancer Biol. Ther 16, 1802–1811 (2015). [PubMed: 26383051]
5. Thomas DA, Massagué J, TGF-β directly targets cytotoxic T cell functions during tumor evasion of immune surveillance. Cancer Cell 8, 369–380 (2005). [PubMed: 16286245]
6. Pickup M, Novitskiy S, Moses HL, The roles of TGFβ in the tumour microenvironment. Nat. Rev. Cancer 13, 788–799 (2013). [PubMed: 24132110]
7. Gorelik L, Flavell RA, Immune-mediated eradication of tumors through the blockade of transforming growth factor-β signaling in T cells. Nat. Med 7, 1118–1122 (2001). [PubMed: 11590434]
8. Shevach EM, Mechanisms of foxp3^{+} T regulatory cell-mediated suppression. Immunity 30, 636–645 (2009). [PubMed: 19464986]
9. Tauriello DVF, Palomo-Ponce S, Stork D, Berenguer-Llergo A, Badia-Ramentol J, Iglesias M, Sevillano M, Ibiza S, Cañellas A, Hernando-Momblona X, Byrom D, Matarin JA, Calon A, Rivas EI, Nebreda AR, Riera A, Attolini CS-O, Batlle E, TGFβ drives immune evasion in genetically reconstituted colon cancer metastasis. Nature 554, 538–543 (2018). [PubMed: 29443964]
10. Papageorgis P, Stylianopoulos T, Role of TGFβ in regulation of the tumor microenvironment and drug delivery (review). Int. J. Oncol 46, 933–943 (2015). [PubMed: 25573346]
11. Cui W, Fowlis DJ, Bryson S, Duffie E, Ireland H, Balmain A, Akhurst RJ, TGFβ1 inhibits the formation of benign skin tumors, but enhances progression to invasive spindle carcinomas in transgenic mice. Cell 86, 531–542 (1996). [PubMed: 8752208]
12. Padua D, Massagué J, Roles of TGFβ in metastasis. Cell Res. 19, 89–102 (2009). [PubMed: 19050696]
13. Poniatowski LA, Wojdasiewicz P, Gasik R, Szukiewicz D, Transforming growth factor Beta family: Insight into the role of growth factors in regulation of fracture healing biology and potential clinical applications. Mediators Inflamm. 2015, 137823 (2015). [PubMed: 25709154]
14. Gentry LE, Lioubin MN, Purchio AF, Marquardt H, Molecular events in the processing of recombinant type 1 pre-pro-transforming growth factor beta to the mature polypeptide. Mol. Cell. Biol 8, 4162–4168 (1988). [PubMed: 3185545]
15. Rifkin DB, Latent transforming growth factor-β (TGF-β) binding proteins: Orchestrators of TGF-β availability. J. Biol. Chem 280, 7409–7412 (2005). [PubMed: 15611103]
16. Shi M, Zhu J, Wang R, Chen X, Mi L, Walz T, Springer TA, Latent TGF-β structure and activation. Nature 474, 343–349 (2011). [PubMed: 21677751]
17. Wang R, Zhu J, Dong X, Shi M, Lu C, Springer TA, GARP regulates the bioavailability and activation of TGFβ. Mol. Biol. Cell 23, 1129–1139 (2012). [PubMed: 22278742]
18. Liénart S, Stockis J, Dedobbeleer O, Lucas S, Targeting immunosuppression by Tregs with monoclonal antibodies against GARP. Oncoimmunology 5, e1074379 (2016). [PubMed: 27141368]
19. Stockis J, Colau D, Coulie PG, Lucas S, Membrane protein GARP is a receptor for latent TGF-β on the surface of activated human Treg. Eur. J. Immunol 39, 3315–3322 (2009). [PubMed: 19750484]
20. Metelli A, Wu BX, Fugle CW, Rachidi S, Sun S, Zhang Y, Wu J, Tomlinson S, Howe PH, Yang Y, Garrett-Mayer E, Liu B, Li Z, Surface expression of TGFβ docking receptor GARP promotes oncogenesis and immune tolerance in breast cancer. Cancer Res. 76, 7106–7117 (2016). [PubMed: 27913437]

21. Tran DQ, Andersson J, Wang R, Ramsey H, Unutmaz D, Shevach EM, GARP (LRRC32) is essential for the surface expression of latent TGF-β on platelets and activated FOXP3^{+} regulatory T cells. Proc. Natl. Acad. Sci. U.S.A 106, 13445–13450 (2009). [PubMed: 19651619]
22. Dedobbeleer O, Stockis J, van der Woning B, Coulie PG, Lucas S, Cutting Edge: Active TGF-β1 released from GARP/TGF-β1 complexes on the surface of stimulated human B lymphocytes increases class-switch recombination and production of IgA. J. Immunol 199, 391–396 (2017). [PubMed: 28607112]
23. Wallace CH, Wu BX, Salem M, Ansa-Addo EA, Metelli A, Sun S, Gilkeson G, Shlomchik MJ, Liu B, Li Z, B lymphocytes confer immune tolerance via cell surface GARP-TGF-β complex. JCI Insight 3, pii: 99863 (2018). [PubMed: 29618665]
24. Salem M, Wallace C, Velegraki M, Li A, Ansa-Addo E, Metelli A, Kwon H, Riesenberg B, Wu B, Zhang Y, Guglietta S, Sun S, Liu B, Li Z, GARP dampens cancer immunity by sustaining function and accumulation of regulatory T cells in the colon. Cancer Res. 79, 1178–1190 (2019). [PubMed: 30674536]
25. Rachidi S, Metelli A, Riesenberg B, Wu BX, Nelson MH, Wallace C, Paulos CM, Rubinstein MP, Garrett-Mayer E, Hennig M, Bearden DW, Yang Y, Liu B, Li Z, Platelets subvert T cell immunity against cancer via GARP-TGFβ axis. Sci. Immunol 2, eaai7911 (2017). [PubMed: 28763790]
26. Qian WJ, Monroe ME, Liu T, Jacobs JM, Anderson GA, Shen Y, Moore RJ, Anderson DJ, Zhang R, Calvano SE, Lowry SF, Xiao W, Moldawer LL, Davis RW, Tompkins RG, Camp II DG, Smith RD; Inflammation and the Host Response to Injury Large Scale Collaborative Research Program, Quantitative proteome analysis of human plasma following in vivo lipopolysaccharide administration using $^{16}O/^{18}O$ labeling and the accurate mass and time tag approach. Mol. Cell. Proteomics 4, 700–709 (2005). [PubMed: 15753121]
27. Zhang Y, Wu BX, Metelli A, Thaxton JE, Hong F, Rachidi S, Ansa-Addo E, Sun S, Vasu C, Yang Y, Liu B, Li Z, GP96 is a GARP chaperone and controls regulatory T cell functions. J. Clin. Invest 125, 859–869 (2015). [PubMed: 25607841]
28. Lienart S, Merceron R, Vanderaa C, Lambert F, Colau D, Stockis J, van der Woning B, De Haard H, Saunders M, Coulie PG, Savvides SN, Lucas S, Structural basis of latent TGF-β1 presentation and activation by GARP on human regulatory T cells. Science 362, 952–956 (2018). [PubMed: 30361387]
29. Kozakov D, Beglov D, Bohnuud T, Mottarella SE, Xia B, Hall DR, Vajda S, How good is automated protein docking? Proteins 81, 2159–2166 (2013). [PubMed: 23996272]
30. Gauthy E, Cuende J, Stockis J, Huygens C, Lethé B, Collet J-F, Bommer G, Coulie PG, Lucas S, GARP is regulated by miRNAs and controls latent TGF-β1 production by human regulatory T cells. PLOS ONE 8, e76186 (2013). [PubMed: 24098777]
31. Monroe DM, Hoffman M, Roberts HR, Platelets and thrombin generation. Arterioscler. Thromb. Vasc. Biol 22, 1381–1389 (2002). [PubMed: 12231555]
32. Wolberg AS, Campbell RA, Thrombin generation, fibrin clot formation and hemostasis. Transfus. Apher. Sci 38, 15–23 (2008). [PubMed: 18282807]
33. Zemer-Wassercug N, Haim M, Leshem-Lev D, Orvin KL, Vaduganathan M, Gutstein A, Kadmon E, Mager A, Kornowski R, Lev EL, The effect of dabigatran and rivaroxaban on platelet reactivity and inflammatory markers. J. Thromb. Thrombolysis 40, 340–346 (2015). [PubMed: 26184605]
34. DeFeo K, Hayes C, Chernick M, Van Ryn J, Gilmour SK, Use of dabigatran etexilate to reduce breast cancer progression. Cancer Biol. Ther 10, 1001–1008 (2010). [PubMed: 20798593]
35. Dahmani A, Delisle J-S, TGF-β in T cell biology: Implications for cancer immunotherapy. Cancers (Basel) 10, E194 (2018). [PubMed: 29891791]
36. Chen X, Oppenheim JJ, Resolving the identity myth: Key markers of functional CD4^{+}FoxP3^{+} regulatory T cells. Int. Immunopharmacol 11, 1489–1496 (2011). [PubMed: 21635972]
37. Terabe M, Robertson FC, Clark K, De Ravin E, Bloom A, Venzon DJ, Kato S, Mirza A, Berzofsky JA, Blockade of only TGF-β 1 and 2 is sufficient to enhance the efficacy of vaccine and PD-1 checkpoint blockade immunotherapy. Oncoimmunology 6, e1308616 (2017). [PubMed: 28638730]

38. Fernandes CJ, Morinaga LTK, Alves JL Jr., Castro MA, Calderaro D, C. V. P. Jardim, R. Souza, Cancer-associated thrombosis: The when, how and why. Eur. Respir. Rev 28, 180119 (2019). [PubMed: 30918022]
39. Gieseler F, Lühr I, Kunze T, Mundhenke C, Maass N, Erhart T, Denker M, Beckmann D, Tiemann M, Schulte C, Dohrmann P, Cavaillé F, Godeau F, Gespach C, Activated coagulation factors in human malignant effusions and their contribution to cancer cell metastasis and therapy. Thromb. Haemost 97, 1023–1030 (2007). [PubMed: 17549306]
40. Wang AS-S, Chen C-H, Chou Y-T, Pu Y-S, Perioperative changes in TGF-β1 levels predict the oncological outcome of cryoablation-receiving patients with localized prostate cancer. Cryobiology 73, 63–68 (2016). [PubMed: 27256663]
41. Erpenbeck L, Schon MP, Deadly allies: The fatal interplay between platelets and metastasizing cancer cells. Blood 115, 3427–3436 (2010). [PubMed: 20194899]
42. Xue T-C, Ge N-L, Xu X, le F, Zhang B-H, Wang Y-H, High platelet counts increase metastatic risk in huge hepatocellular carcinoma undergoing transarterial chemoembolization. Hepatol. Res 46, 1028–1036 (2016). [PubMed: 26776560]
43. Sylman JL, Mitrugno A, Tormoen GW, Wagner TH, Mallick P, McCarty OJT, Platelet count as a predictor of metastasis and venous thromboembolism in patients with cancer. Converg. Sci. Phys. Oncol 3, 023001 (2017). [PubMed: 29081989]
44. Palta S, Saroa R, Palta A, Overview of the coagulation system. Indian J. Anaesth 58, 515–523 (2014). [PubMed: 25535411]
45. Stockis J, Liénart S, Colau D, Collignon A, Nishimura SL, Sheppard D, Coulie PG, Lucas S, Blocking immunosuppression by human Tregs in vivo with antibodies targeting integrin αVβ8. Proc. Natl. Acad. Sci. U.S.A 114, E10161–E10168 (2017). [PubMed: 29109269]
46. Lee CJ, Ansell JE, Direct thrombin inhibitors. Br. J. Clin. Pharmacol 72, 581–592 (2011). [PubMed: 21241354]
47. Vinholt PJ, Nielsen C, Söderström AC, Brandes A, Nybo M, Dabigatran reduces thrombin-induced platelet aggregation and activation in a dose-dependent manner. J. Thromb. Thrombolysis 44, 216–222 (2017). [PubMed: 28580515]
48. Shi K, Damhofer H, Daalhuisen J, ten Brink M, Richel DJ, Spek CA, Dabigatran potentiates gemcitabine-induced growth inhibition of pancreatic cancer in mice. Mol. Med 23, 13–23 (2017). [PubMed: 28182192]
49. Kawase T, Okuda K, Wolff LF, Yoshie H, Platelet-rich plasma-derived fibrin clot formation stimulates collagen synthesis in periodontal ligament and osteoblastic cells in vitro. J. Periodontol 74, 858–864 (2003). [PubMed: 12886997]
50. Kopp H-G, Placke T, Salih HR, Platelet-derived transforming growth factor-β down-regulates NKG2D thereby inhibiting natural killer cell antitumor reactivity. Cancer Res. 69, 7775–7783 (2009). [PubMed: 19738039]
51. Haselmayer P, Grosse-Hovest L, von Landenberg P, Schild H, Radsak MP, TREM-1 ligand expression on platelets enhances neutrophil activation. Blood 110, 1029–1035 (2007). [PubMed: 17452516]
52. Philippe C, Philippe B, Fouqueray B, Perez J, Lebret M, Baud L, Protection from tumor necrosis factor-mediated cytolysis by platelets. Am. J. Pathol 143, 1713–1723 (1993). [PubMed: 8256858]
53. Sow HS, Ren J, Camps M, Ossendorp F, ten Dijke P, Combined Inhibition of TGF-β signaling and the PD-L1 immune checkpoint is differentially effective in tumor models. Cell 8, E320 (2019).
54. Holmgaard RB, Schaer DA, Li Y, Castaneda SP, Murphy MY, Xu X, Inigo I, Dobkin J, Manro JR, Iversen PW, Surguladze D, Hall GE, Novosiadly RD, Benhadji KA, Plowman GD, Kalos M, Driscoll KE, Targeting the TGFβ pathway with galunisertib, a TGFβRI small molecule inhibitor, promotes anti-tumor immunity leading to durable, complete responses, as monotherapy and in combination with checkpoint blockade. J. Immunother. Cancer 6, 47 (2018). [PubMed: 29866156]
55. Torre LA, Bray F, Siegel RL, Ferlay J, Lortet-Tieulent J, Jemal A, Global cancer statistics, 2012. CA Cancer J. Clin 65, 87–108 (2015). [PubMed: 25651787]
56. Madu CO, Lu Y, Novel diagnostic biomarkers for prostate cancer. J. Cancer 1, 150–177 (2010). [PubMed: 20975847]

57. Tonry CL, Leacy E, Raso C, Finn SP, Armstrong J, Pennington SR, The role of proteomics in biomarker development for improved patient diagnosis and clinical decision making in prostate cancer. Diagnostics 6, E27 (2016). [PubMed: 27438858]
58. Randow F, Seed B, Endoplasmic reticulum chaperone gp96 is required for innate immunity but not cell viability. Nat. Cell Biol 3, 891–896 (2001). [PubMed: 11584270]
59. Edwards JP, Fujii H, Zhou AX, Creemers J, Unutmaz D, Shevach EM, Regulation of the expression of GARP/latent TGF-β1 complexes on mouse T cells and their role in regulatory T cell and Th17 differentiation. J. Immunol 190, 5506–5515 (2013). [PubMed: 23645881]
60. Tiedt R, Schomber T, Hao-Shen H, Skoda RC, *Pf4-Cre* transgenic mice allow the generation of lineage-restricted gene knockouts for studying megakaryocyte and platelet function in vivo. Blood 109, 1503–1506 (2007). [PubMed: 17032923]
61. Wu S, Hong F, Gewirth D, Guo B, Liu B, Li Z, The molecular chaperone gp96/GRP94 interacts with Toll-like receptors and integrins via its C-terminal hydrophobic domain. J. Biol. Chem 287, 6735–6742 (2012). [PubMed: 22223641]
62. Hartmann FJ, Bernard-Valnet R, Quériault C, Mrdjen D, Weber LM, Galli E, Krieg C, Robinson MD, Nguyen X-H, Dauvilliers Y, Liblau RS, Becher B, High-dimensional single-cell analysis reveals the immune signature of narcolepsy. J. Exp. Med 213, 2621–2633 (2016). [PubMed: 27821550]
63. Nowicka M, Krieg C, Weber LM, Hartmann FJ, Guglietta S, Becher B, Levesque MP, Robinson MD, CyTOF workflow: Differential discovery in high-throughput high-dimensional cytometry datasets. F1000Res 6, 748 (2017). [PubMed: 28663787]
64. Chevrier S, Crowell HL, Zanotelli VRT, Engler S, Robinson MD, Bodenmiller B, Compensation of signal spillover in suspension and imaging mass cytometry. Cell Syst. 6, 612–620.e5 (2018). [PubMed: 29605184]
65. Van Gassen S, Callebaut B, Van Helden MJ, Lambrecht BN, Demeester P, Dhaene T, Saeys Y, FlowSOM: Using self-organizing maps for visualization and interpretation of cytometry data. Cytometry A 87, 636–645 (2015). [PubMed: 25573116]
66. Waterhouse A, Bertoni M, Bienert S, Studer G, Tauriello G, Gumienny R, Heer FT, de Beer TAP, Rempfer C, Bordoli L, Lepore R, Schwede T, SWISS-MODEL: Homology modelling of protein structures and complexes. Nucleic Acids Res. 46, W296–W303 (2018). [PubMed: 29788355]
67. Weber LM, Nowicka M, Soneson C, Robinson MD, diffcyt: Differential discovery in high-dimensional cytometry via high-resolution clustering. Commun. Biol 2, 183 (2019). [PubMed: 31098416]

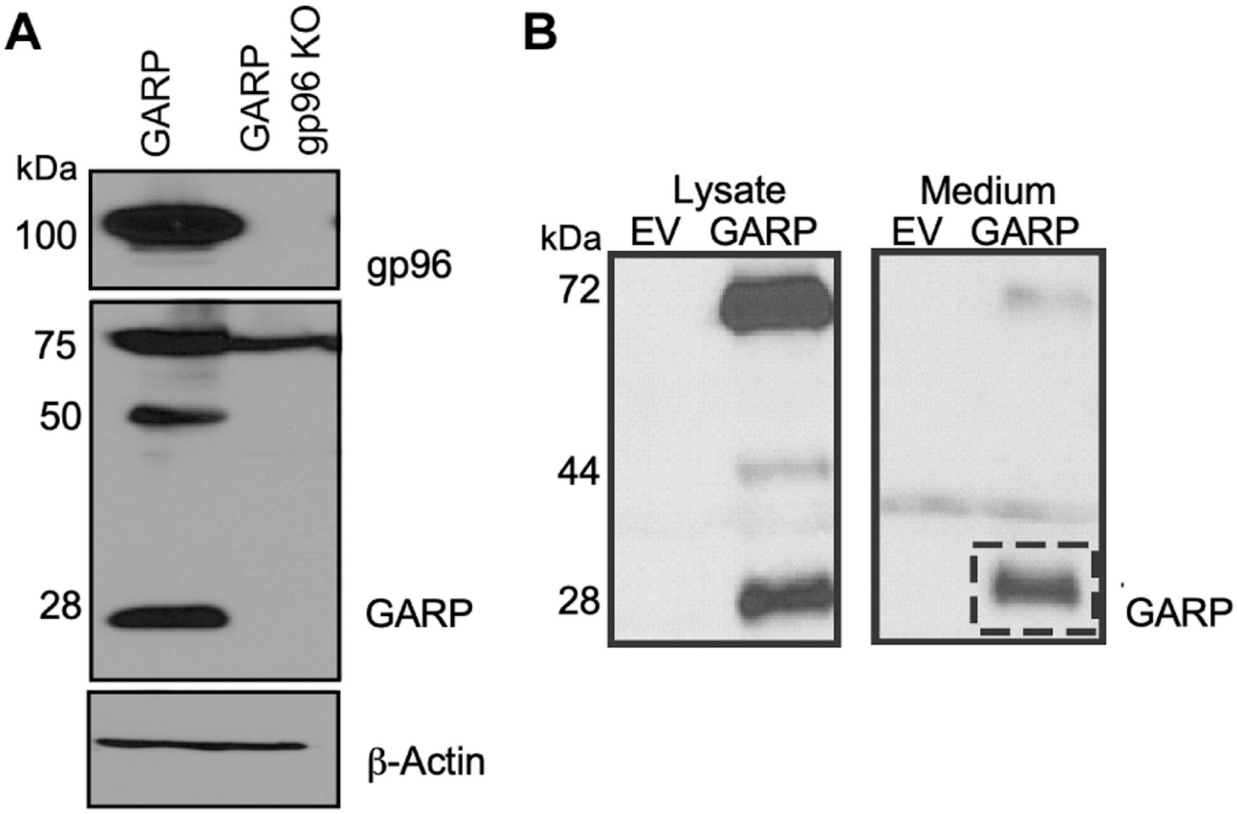

C

MCG51019, isoform CRA_b OS=MUSC musculus GN=Lrrc32 PE=4 SV=1 - [G3XA59_MOUSE]	42.2	1.96
A3	Sequence	#PSMS
High	LRTLSAENSLTR	4
High	TLSLAENSTR	10

Fig. 1. N-terminal fragment of mouse GARP is shed from the cell surface.

(**A**) Western blot analysis of GARP in the total cell lysate of WT and gp96 KO pre–B cells. Cell lysates were analyzed by using antibodies against mouse GARP and mouse gp96. Reducing condition gel was used. (**B**) Parallel Western blot analysis of cell lysates and conditioned medium of WT pre–B cells expressing GARP or control vector. Reducing condition gel was used. EV, empty vector. (A) and (B) are representative of more than three independent biological experiments. (**C**) Mass spectrometry analysis of the fragment present in the conditioned medium of pre–B cells expressing GARP. #PSMS, number of identified sequences (peptide spectrum matches). G3XA59 is UniProtKB for GARP.

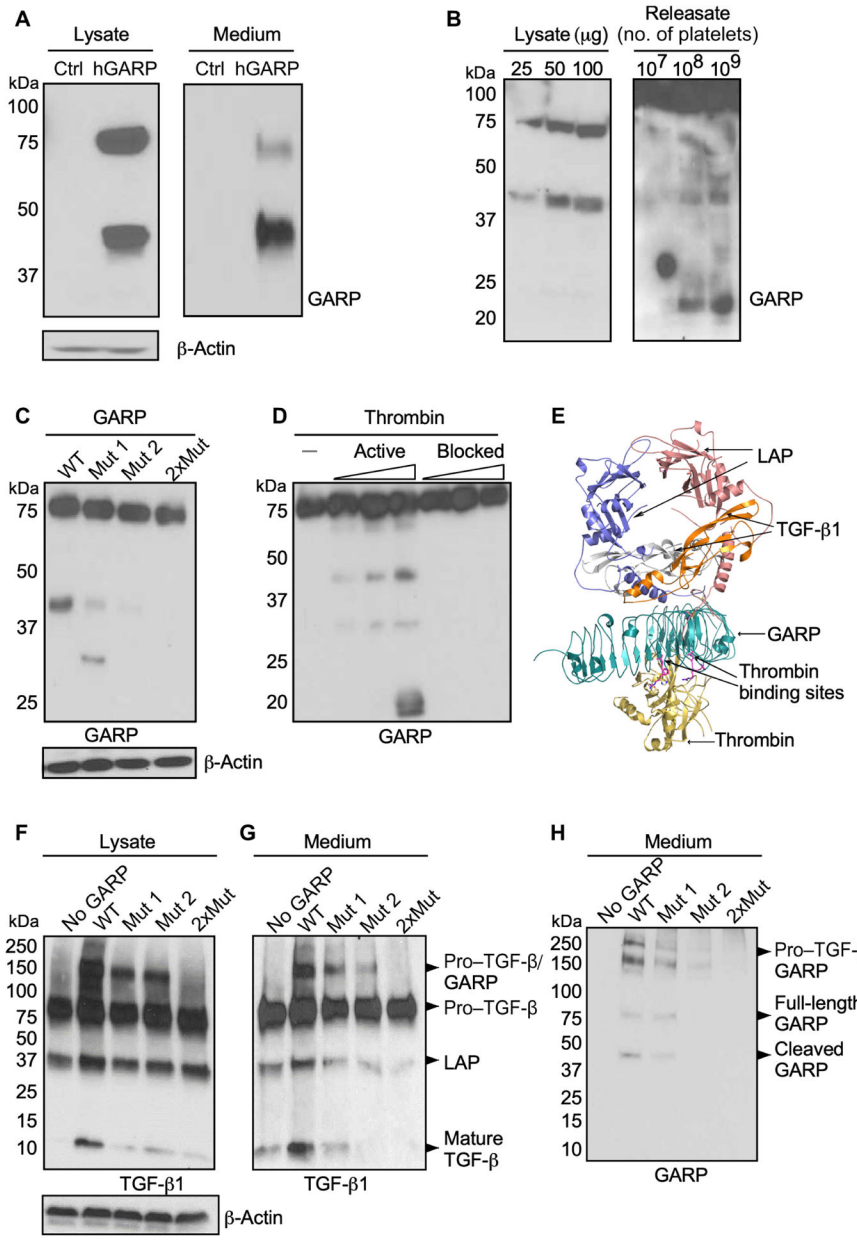

Fig. 2. Thrombin is responsible for cleavage of human GARP.

(**A**) Western blot analysis of cell lysate and conditioned medium of HEK293 cells expressing human GARP (hGARP) or a control (Ctrl) empty vector. Reducing condition gel was used. β-Actin was used as a loading control. (**B**) Western blot analysis of human platelet lysate (25, 50, and 100 μg) and the releasate obtained from increasing concentrations of platelets (10^7, 10^8, and 10^9 per ml). Reducing condition gel was used. (**C**) Western blot analysis of HEK293 cells expressing wild-type (WT) human GARP or GARP with single (Mut 1 or Mut 2) or both thrombin binding sites mutated (2xMut). Reducing condition gel was used. (**D**) Western blot analysis of 1 μg of recombinant human GARP digested with increasing concentration of human thrombin with active (left) and blocked (right) activity. Reducing condition gel was used. (**E**) Representative molecular model of a thrombin, GARP,

and LTGF-β1 complex showing that thrombin can bind GARP on the surface opposite of LTGF-β1. Western blot analysis for TGF-β1 in cell lysate (**F**) and the conditioned medium (**G**) of HEK293 cells expressing TGF-β1 only or TGF-β1 in combination with WT or mutant GARP. (**H**) Same samples as in (G) were immunoblotted for GARP. Nonreducing condition gel was used for (F) to (H). At least three independent experiments were performed with similar findings.

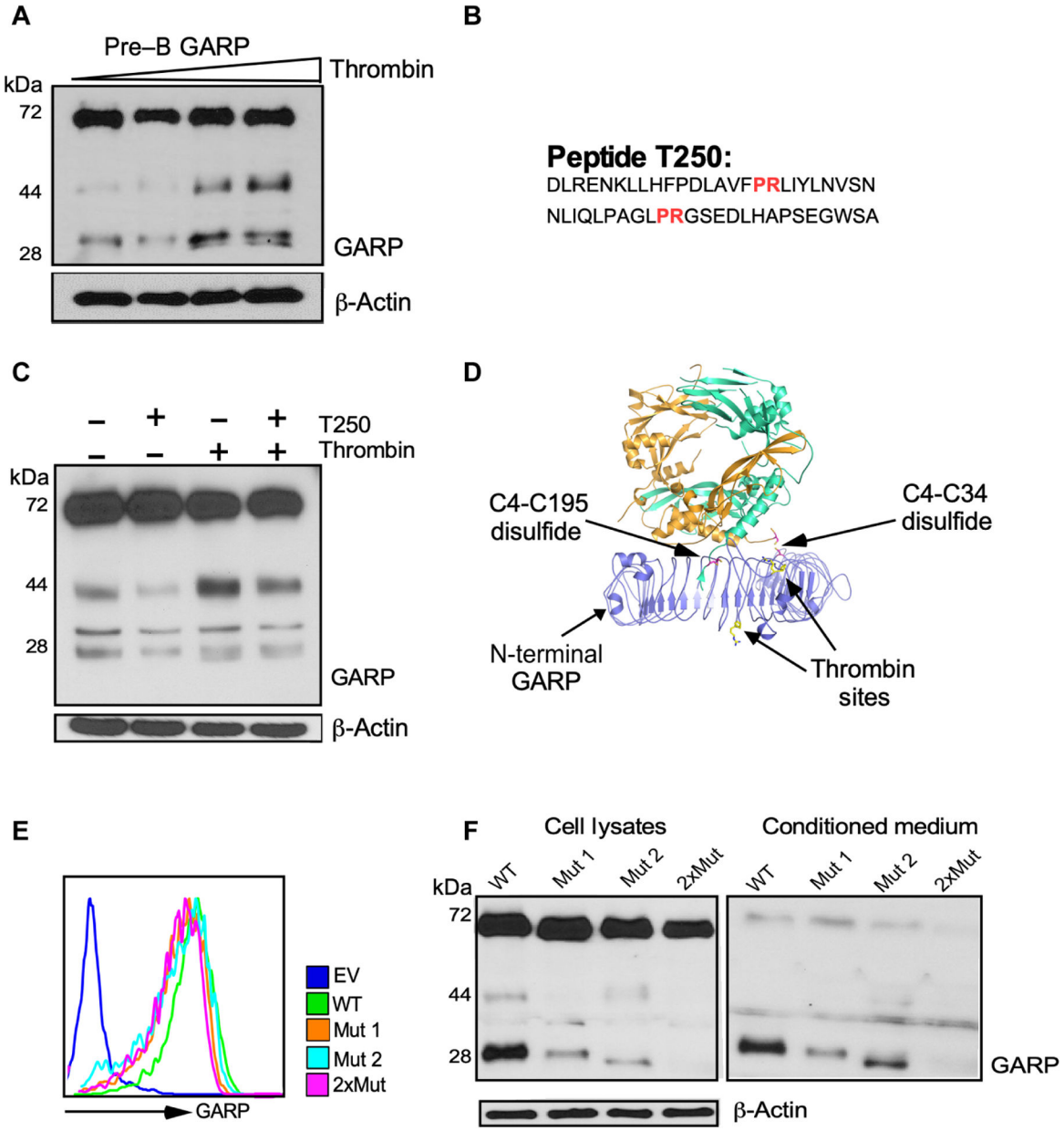

Fig. 3. Molecular and biochemical mapping demonstrates mouse cell surface GARP as a thrombin substrate.

(**A**) GARP-expressing pre–B cells were digested with increasing concentrations of thrombin (0, 1, 2, and 4 μg in 25 μl), followed by Western blot analysis. Reducing condition gel was used. (**B**) Sequence of GARP fragments containing the two PR thrombin binding sites, T250. (**C**) Western blotting analysis of GARP-expressing pre–B cells digested with 4 μg of thrombin in the presence or absence of 4 μg of T250. Reducing condition gel was used. (**D**) Structural model of the mouse GARP/LTGF-β1 interaction. (**E**) Flow cytometry analysis of cell surface GARP on WT pre–B cells or pre–B cells expressing various forms of mutant GARP or empty vector. (**F**) Western blot analysis of GARP in whole-cell lysates and

conditioned medium of pre–B cells expressing WT or mutant GARP. Reducing condition gel electrophoresis was performed.

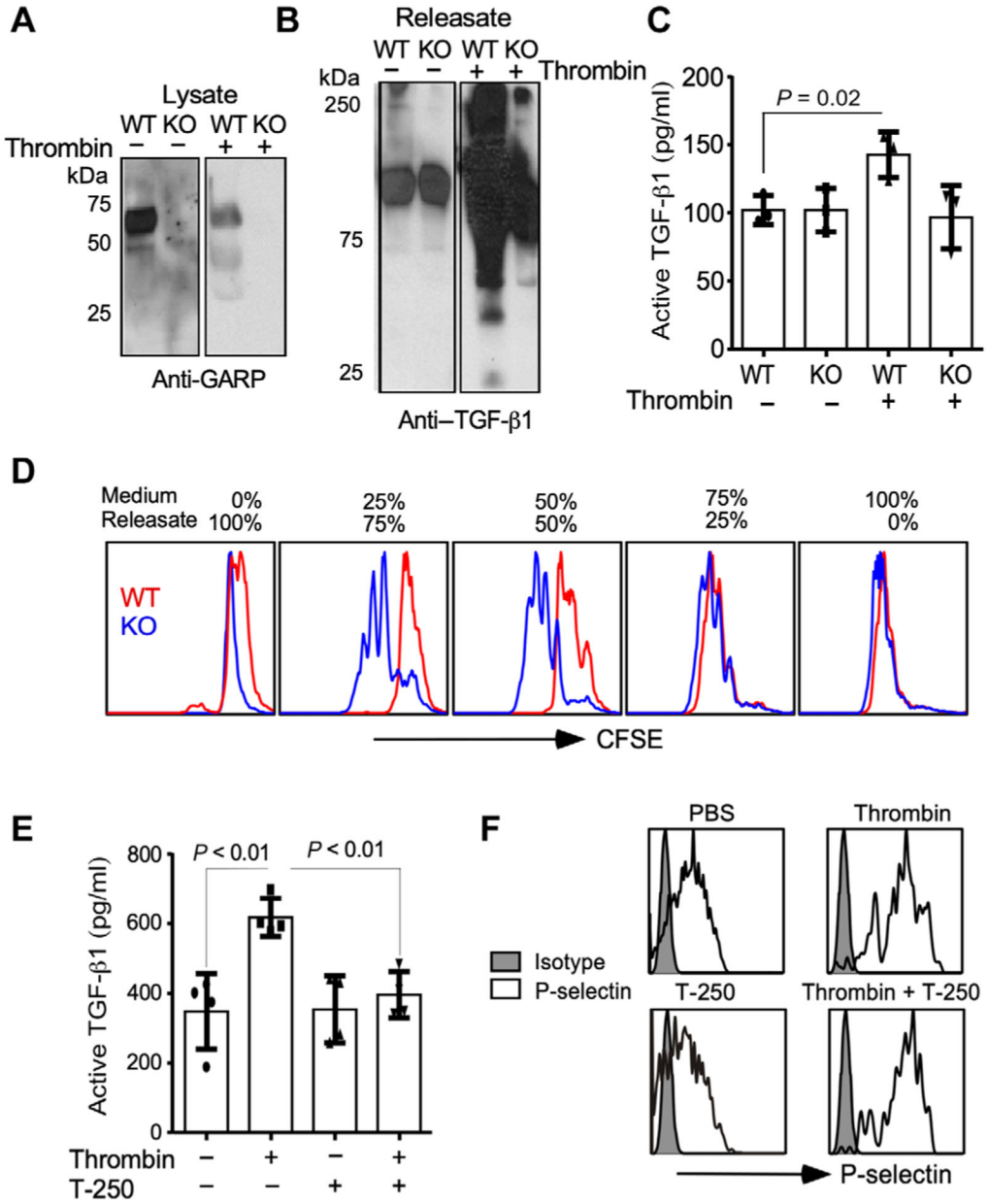

Fig. 4. Thrombin cleavage of mouse GARP liberates mature TGF-β1.

(**A**) Mouse WT and GARP KO platelets were collected and stimulated with thrombin or not. Western blot analysis was performed on platelet lysate using anti-GARP antibody. Reducing condition gel was used. (**B**) Platelet releasate from WT and GARP KO platelets was obtained with and without thrombin stimulation and analyzed by Western blot under nonreducing and nondenaturing conditions using anti–TGF-β1 antibody. Nonreducing condition gel was used. (**C**) Platelet releasate from WT and GARP KO platelets was obtained with and without thrombin stimulation, and active TGF-β1 was quantified by ELISA. Data shown as means ± SD ($n = 3$). (**D**) Mouse splenocytes were labeled with carboxyfluorescein diacetate succinimidyl ester (CFSE), followed by activation with anti-CD3ε/CD28 and interleukin-2 for 3 days in the presence of different concentrations of

platelet releasate. $CD4^+$ lymphocytes were then analyzed by flow cytometry. (**E**) WT platelets were untreated or stimulated with the indicated conditions. Platelet releasate was collected, and active TGF-β1 was quantified by ELISA. Data shown as means ± SD ($n = 4$). (**F**) Flow cytometry analysis of P-selectin expression in mouse platelets stimulated in the presence of thrombin and/or T250 peptide.

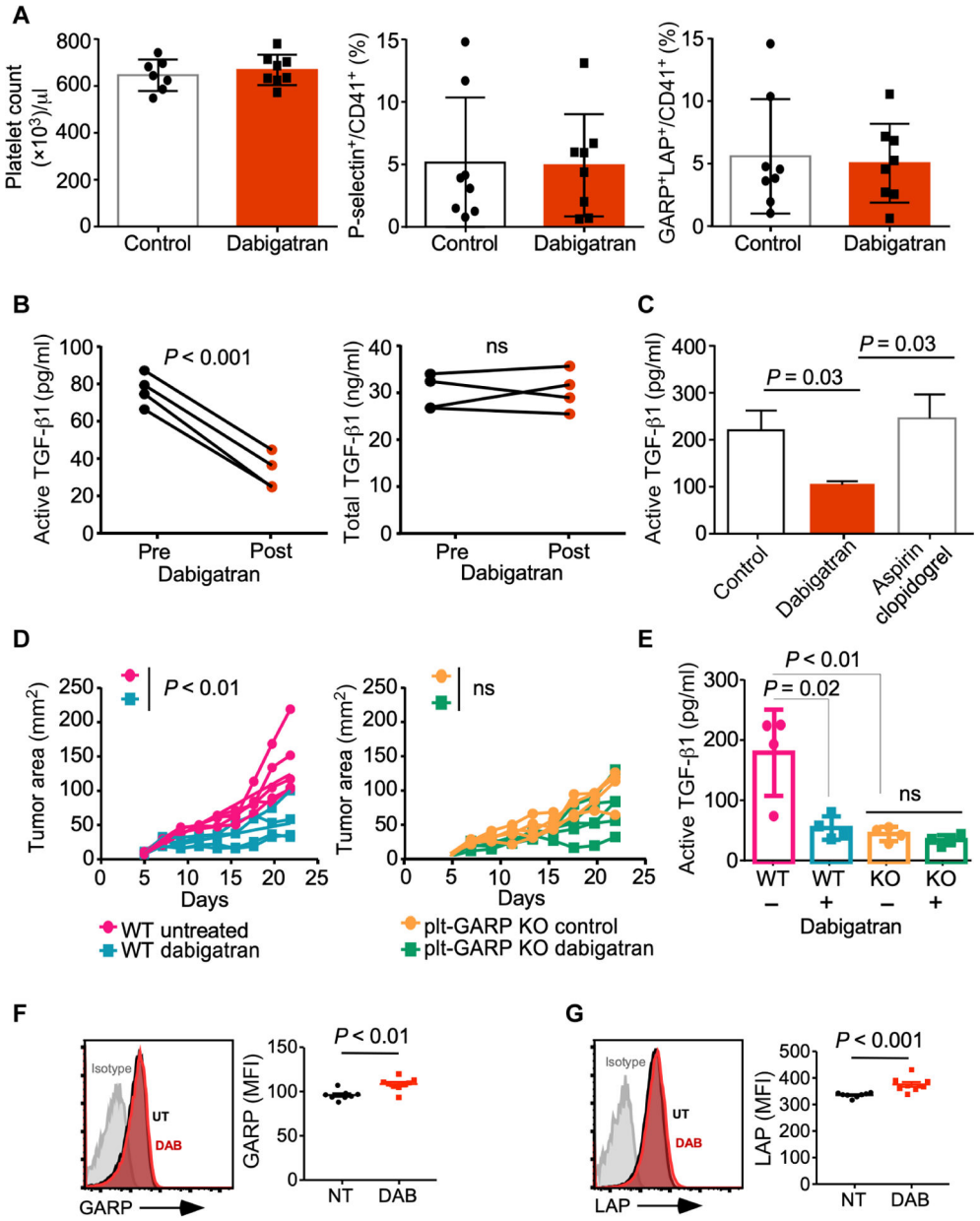

Fig. 5. Cleavage of platelet GARP mediates serum LTGF-β1 activation and tumor progression.

Female C57BL/6 mice were treated for 1 week with dabigatran etexilate, and blood was drawn and analyzed. (**A**) Platelet number and activation status. (**B**) Serum active TGF-β1 (as a measurement of active TGF-β1 release from blood clots) and total TGF-β1 quantified by ELISA. ns, not significant. (**C**) C57BL/6 female mice were treated for 1 week with dabigatran etexilate or clopidogrel and aspirin or left untreated. Serum active TGF-β1 was evaluated by ELISA. Mice with WT and GARP KO platelets were challenged with MC38 cells and treated with dabigatran etexilate or left untreated. (**D**) Tumor area. (**E**) Serum active TGF-β1 from MC38-bearing mice was evaluated by ELISA. (**F** and **G**) Dabigatran treatment enhances GARP and LAP expression on circulating platelets. WT mice were treated with dabigatran (DAB; 3 mg per mouse) or sham control (UT) daily for 1 week.

Platelets were purified and analyzed by flow cytometry for surface expression of (F) GARP or (G) LAP. MFI, mean fluorescent intensity. Data presented as means ± SEM, $n = 8$ to 10 mice per group. Two-tailed, paired Student's t test was used in (B), (F), and (G); two-tailed, independent Student's t test was used in (C) and (E); and repeated measurement two-way ANOVA was performed in (D).

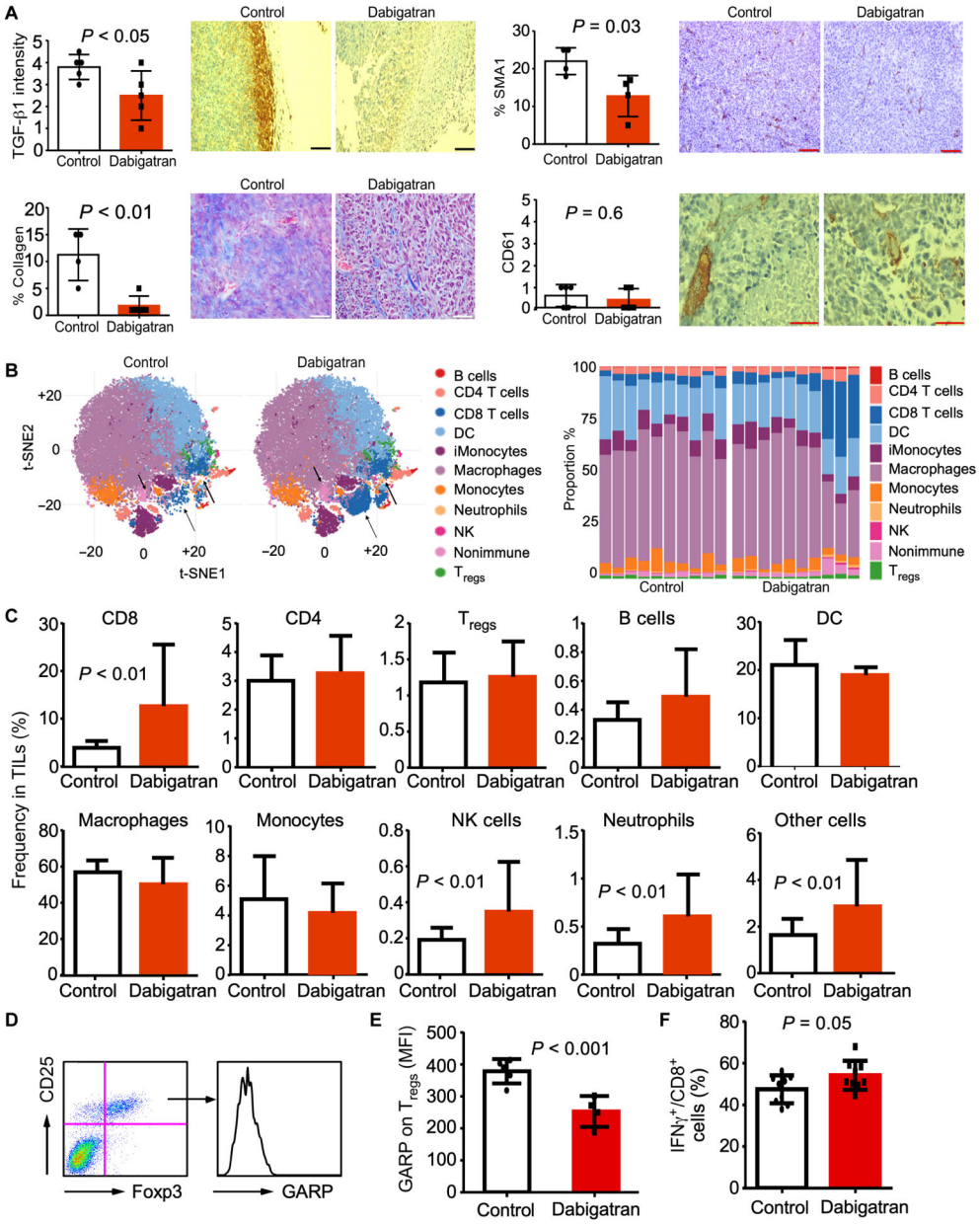

Fig. 6. Cleavage of platelet GARP supports TGF-β1–mediated immune evasion in the tumor microenvironment.

(**A**) Representative images with relative expression intensity of TGF-β1, collagen, SMA1, and CD61 in MC38 tumors collected from WT mice treated with dabigatran etexilate for 3 weeks or left untreated. Each symbol represents an individual mouse. Scale bars, 100 μm (TGF-β1 and SMA1) and 50 μm (collagen and CD61). (**B** and **C**) Mass cytometry analysis of intratumoral cell populations isolated from C57BL/6 mice (n = 10 per group) subcutaneously injected with MC38 and treated daily with dabigatran etexilate for 3 weeks. (B) The combined dataset was down-sampled to 2500 cells per sample for a total of 50,000 cells and subjected to dimensionality reduction using the t-distributed stochastic neighbor embedding (t-SNE) algorithm with the sample-specific composition in tumors of dabigatran etexilate–treated or untreated mice. Relative distribution of immune and nonimmune cells is

indicated in the right. $CD8^+$ T cells, NK cells, and neutrophils are indicated by arrows. (C) Statistical comparison of the frequencies of immune cell populations. DC, dendritic cells; TILs, tumor-infiltrating lymphocytes. (**D**) Representative image of GARP staining in regulatory T cells (T_{regs}). (**E**) Flow cytometry analysis of the MFI of GARP expression on T_{regs} isolated from MC38 tumors in mice treated with dabigatran and control. (**F**) Tumor-infiltrating $CD8^+$ T cells were treated with pyridine-2-aldoxime methiodide/ionomycin for 4 hours, followed by intracellular staining of IFNγ. Two-tailed, independent Student's *t* test was used in (A) and (E); adjusted *P* value based on computational framework diffcyt (67) was used in (C).

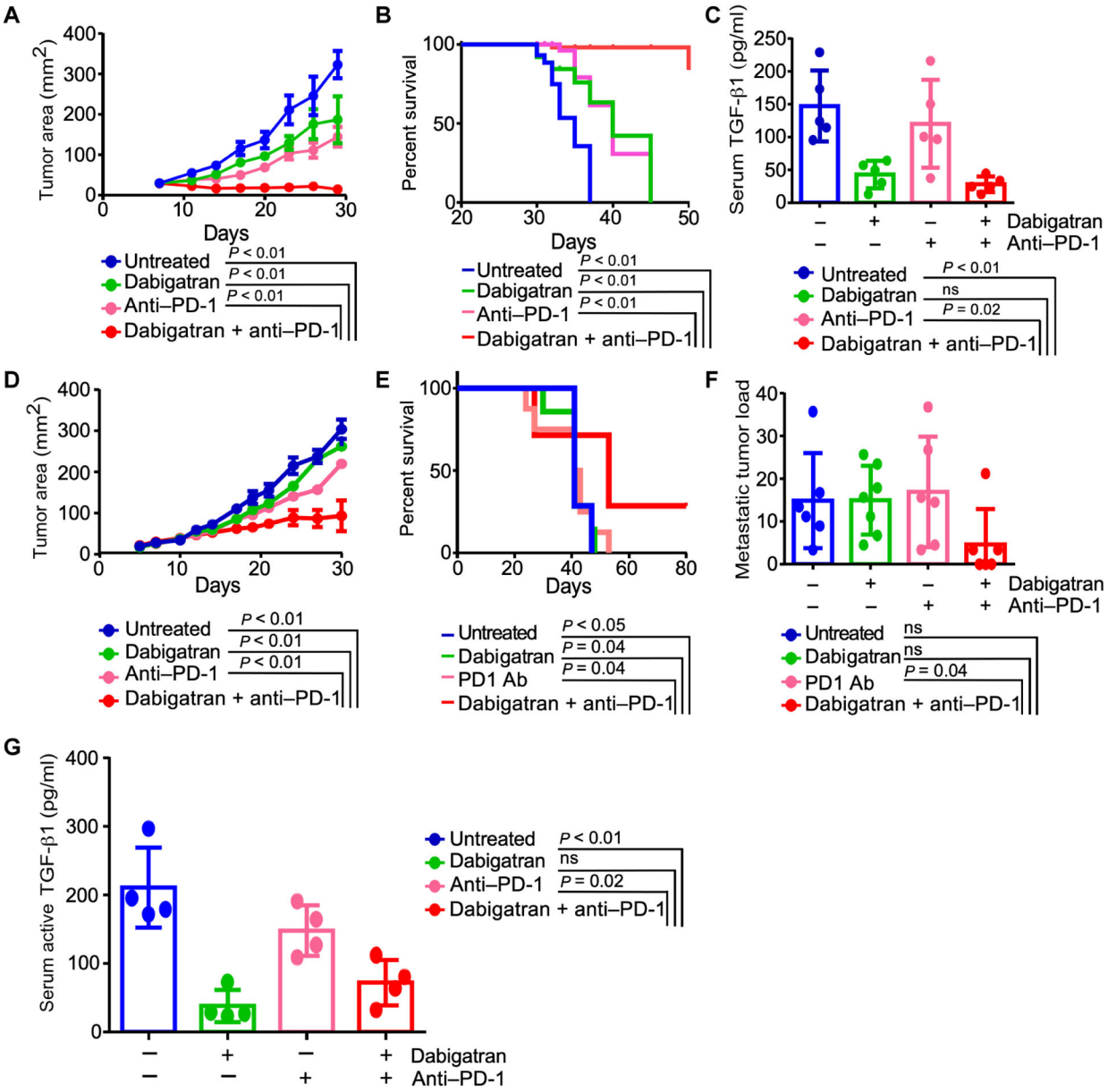

Fig. 7. Blocking platelet GARP cleavage enhances immune checkpoint blockade therapy of cancer.

WT C57BL/6 mice were injected with MC38 colon cancer cells and left untreated or treated with dabigatran etexilate alone, PD-1 blocking antibody (Ab) alone, or combination of both. (**A**) Tumor growth curves. (**B**) Mouse survival. (**C**) Serum active TGF-β1 measured by ELISA. BALB/c female mice were injected into the fourth left mammary fat pad with EMT-6 triple-negative breast cancer cells and treated with dabigatran etexilate alone, PD-1 blocking antibody alone, or both. (**D**) Tumor growth curves. (**E**) Mouse survival. (**F**) Metastatic burden in the lungs. (**G**) Serum active TGF-β1 in EMT-6–bearing BALB/c female mice treated with indicated conditions. Repeated measurement two-way ANOVA was performed in (A), log-rank (Mantel-Cox) was performed in (B) and (E), and two-tailed, independent Student's *t* test was used in (F). The experiment with MC38 tumor models was

performed three times, and EMT-6 was performed two times. For each experiment, six to eight animals per group were used. All *P* values reflect comparison to the combination group (dabigatran plus anti–PD-1).

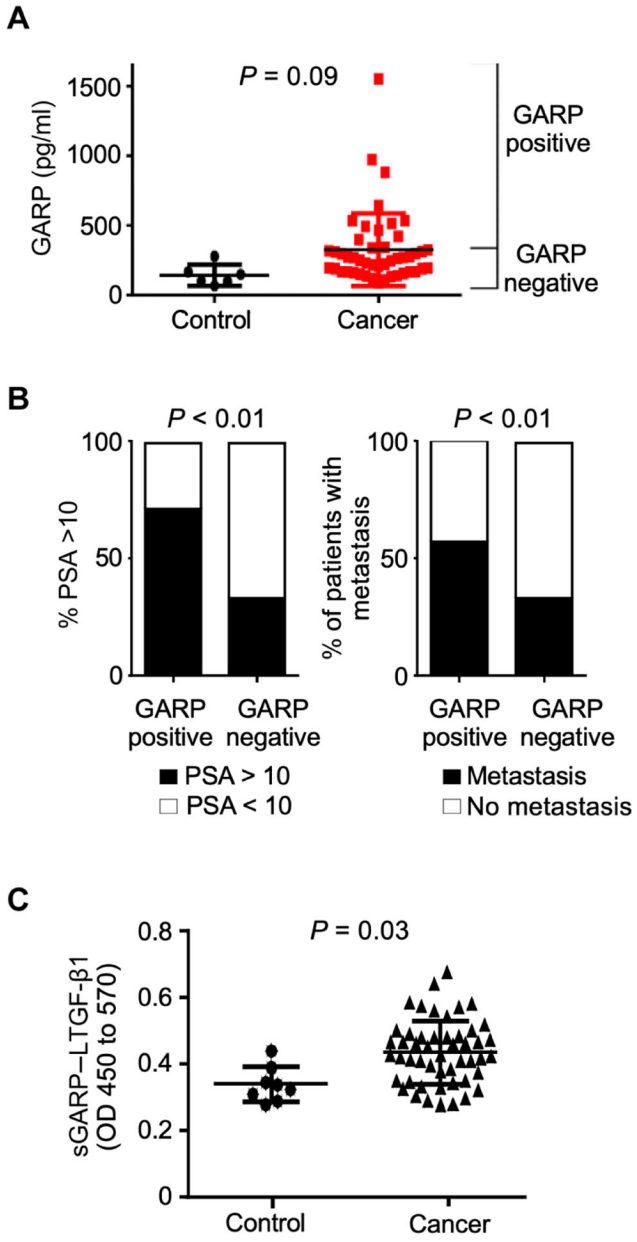

Fig. 8. Both sGARP and sGARP–LTGF-β1 complex are present in patients with cancer.

(**A**) sGARP was detected by ELISA in plasma samples collected from patients with prostate cancer and healthy controls. (**B**) Correlation analysis between GARP-positive or GARP-negative plasma samples and PSA concentration greater or less than 10 ng/ml (left) or the presence of metastasis (right). (**C**) GARP–LTGF-β1 sandwich ELISA performed on plasma samples collected in heparin-coated tubes from patients with prostate cancer and healthy controls. OD, optical density. Two-tailed, independent Student's *t* test was used in (A) and (C). χ^2 test was used in (B).